STRUCTURE OF SILK FIBROIN NANOPARTICLES: CHARACTERIZATION OF HYDROPHOBIC PATCHES

Mammedzade A.M., Mammadova Ay.J., Gasymov O.K.
Institute of Biophysics of Azerbaijan National Academy of Sciences
Z. Khalilov, 117, Baku, AZ1171, Azerbaijan; e-mail: ogassymo@g.ucla.edu; oktaygasimov@gmail.com
Received 13.07.2022. DOI: 10.29039/rusjbpc.2022.0513

Abstract. Nanoparticles are extensively used in various areas of industry. Among different nanoparticles, protein nanoparticles complexed with a wide range of drugs have a great potential for biomedical applications. Silk fibroin exhibits good biocompatibility properties and, therefore, is a good raw material for a wide variety of applications. In this study, structure and hydrophobic patch formation were studied in nanoparticles fabricated from silk fibroin. Far-UV circular dichroism spectroscopy and birefringence observed in a polarized microscope with Congo red staining indicate that fibroin nanoparticles are composed of small amyloid domains. Steady-state and time-resolved fluorescence of ANS revealed two hydrophobic patch formations. Decay-associated spectra of ANS bound to these patches show two species with lifetimes of about 4.2 ns and 14.8 ns. Dissociation constants for ANS complex formation for these patches are 8.3±0.4 μM and 5.9±0.3 μM, respectively. Acrylamide fluorescence quenching shows that solvent accessibility to native Trp residues is significantly decreased during fibroin nanoparticle formation. Data indicate that nanoparticles fabricated from fibroin are a good candidate for drug delivery applications.
Key words*: protein nanoparticles, steady-state and time-resolved fluorescence, ANS fluorescence, hydrophobic patches.*

INTRODUCTION

Protein nanoparticles (pNP) are widely used for drug delivery in the treatment of various diseases. By controlling the parameters, such as size, properties of hydrophobic patches, etc., pNPs can be tuned for drug delivery to specific organs. Among various nanoparticle systems, pNPs have several benefits for drug delivery applications. Many properties of pNP, such as the possibility of size control, biocompatibility, low toxicity, ease of surface modification, etc., make them very attractive for medical applications [1]. Most of the drugs, particularly anticancer agents, are hydrophobic and rely on a special delivery system for disease treatments. Dose-limiting toxicity of many anticancer agents is significantly improved by using protein-formulated nanoparticle systems [2].

Generally, pNP formulation employs a desolvation process. It has been shown that the size of pNPs mainly depends on the amount of used desolvating agents. Heat treatment under the denaturing conditions influences the solubility of pNPs, but not the particle size or amount of functional amino groups [3].

Silk fibroin comprises up to 80% of *Bombyx mori* silkworm cocoons and is extensively used as a biomaterial with excellent properties, such as biocompatibility, high mechanical strength, controllable degradation, etc. [4]. Fibroin consists of two polypeptide chains, a heavy (~390 kDa) and light (~26 kDa), which are covalently linked by a disulfide bond. The heavy chain contains four regions, the crystalline (GAGAGS sequence motif), two semicrystalline (GAGAGY, GAGAGV and GAGAGVGY sequence motifs) and amorphous (contains bulky and aromatic side chains) [5]. Fibroin is composed of about 60% crystalline and 40% amorphous parts. Freshly dissolved aqueous solutions of fibroin adopt random coil confirmation that shows the time-dependent conformational transition to beta-structure. This structural transition strongly depends on temperature and is accompanied by protein aggregation [6]. Spectroscopic studies indicate that fibroin aggregates have a beta-amyloid structure and are a good model to examine amyloid formation mechanisms [6].

Fibroin nano- and microparticles have been formulated as a drug delivery system for doxorubicin, a broadly used anti-cancer agent. The system was very effective against MCF-7 and SAOS-2 cell lines in the *in vitro* study [7]. Fibroin nanoparticles (sfNP) possess all features required for biomedical application and are a good candidate for *in vivo* application [7,8]. As mentioned above, a desolvation procedure is used for pNP production, during which significant conformational changes and drug binding site formation occur.

Hydrophobic cavity and/or patch formation have been relatively less studied in pNPs. To fill this gap, we have fabricated sfNP and using various spectroscopic techniques characterized their structure and hydrophobic cavities important for hydrophobic drug delivery. We show that sfNP is composed of small beta-amyloid structures and possesses at least two hydrophobic cavities with distinct characteristics.

MATERIAL AND METHODS

2.1. Silk fibroin purification

Fibroin was purified from silk cocoons of *Bombyx mori* following the conventional procedure described in [9]. Briefly, silk cocoons were cut into small pieces and then boiled in 0.02 M Na_2CO_3 for 30 min. The sericin was washed off with running water and dried in the air. Then, fibroin was dissolved in 9.5 LiBr solution incubating at 60^0C for 4 hours

and then dialyzed (molecular weight cut-off 10 kDa) against deionized water for 2 days at 4^0C. The concentration of fibroin solution was determined by UV absorbance, using ε_{275nm}= 1.064 $cm^{-1}(mg/mL)^{-1}$ [10].

2.2. Preparation of fibroin nanoparticles.

Fibroin nanoparticles were fabricated by jetting the fibroin solution into acetone solution. At the end of the procedure concentration of acetone was above 70% [11]. Dynamic light scattering (Zetasizer Nano ZS, Malvern Instruments, Malvern, UK) measurements operating at λ= 633 nm were used to characterize the size of nanoparticles. After 2 times ultrasonication (20 kHz) procedures with an amplitude of 50% for 30 sec, the solution showed a single peak with a diameter of about 120 nm (data not shown).

2.3. Circular Dichroism spectroscopy

Far-UV CD spectra were recorded using a Chirascan V100 (Applied Photophysics, UK) circular dichroism spectrometer using a step size of 0.5 nm and bandwidth of 1 nm. The path length of the cell was 0.2 mm. To increase the signal/noise ratio, nine spectral scans were averaged. CD spectra were recorded in mdeg and converted to $deg•cm^2•dmol^{-1}$. Secondary structure of sfNP was estimated from far-UV CD spectrum using the DICHROWEB server (http://dichr oweb.cryst.bbk.ac.uk/html/home.shtml) [12,13]. The CDSSTR method [14,15], which showed the best fitting data, was used for the calculation of secondary structure content.

2.4. Congo red binding assay

Congo red (CR) staining experiments were performed to test beta-amyloid formation in fibroin nanoparticles. The dye was freshly prepared in deionized water and concentration was determined using $\varepsilon_{490nm} = 3.3*10^4$ [16]. Solution of fibroin nanoparticles was stained using a 20 μM concentration of CR. The solution was sandwiched between two microscope glass slides for a polarized microscope. The birefringence of CR bound to fibroin nanoparticles was measured through crossed polarizers.

2.5. Fluorescence spectroscopy

Fluorescence spectra and emission decay measurements were recorded using a spectrofluorometer FluoTime 300 (PicoQuant, Germany). For steady-state fluoresce spectra of native Trp residues, the excitation wavelength was chosen 295 nm to prevent contribution from Tyr residues. Nanopulsed LED with 296 nm was selected for the Trp emission decays. The emission decay data were analyzed by multiexponential decay law, using the software of the instrument.

$$I(t) = \sum \alpha_i \exp(-t/\tau_i) \quad (1)$$

Where *I(t)* fluorescence intensity at different times and α_i and τ_i are the normalized preexponential factors and decay time constant, respectively. The intensity-averaged lifetime is $\tau^{av} = \sum f_i \tau_i$, where $f_i = \alpha_i \tau_i / \sum \alpha_j \tau_j$.

Acrylamide quenching experiments of native Trp residues of fibroin in solution and NP forms were performed by both steady-state and time-resolved fluorescence. Quenching with steady-state fluorescence reflects both dynamic and static quenching and, therefore, is described by the following equation:

$$\frac{F_0}{F} = (1 + K_D[Q])(1 + K_S[Q]) \quad (2)$$

F_0 and F represent steady-state fluorescence in the absence and presence of the quencher [Q]. K_D and K_S are dynamic and static quenching constants, respectively. However, only dynamic quenching is involved in quenching with fluorescence lifetimes and is described by

$$\frac{\tau_0}{\tau} = (1 + K_D[Q]) \quad (3)$$

To obtain K_D and K_S values both steady-state and time-resolved fluorescence quenching data were simultaneously fitted to the above-shown equations using Global analysis (OriginPro 16). The K_D was a global parameter. A bimolecular quenching rate constant was calculated as $k_q = K_D/\tau^{av}$. In contrast K_D, k_q does not depend on fluorescence lifetime and is an adequate parameter to measure solvent exposure of the chromophore.

ANS fluorescence was measured with an excitation wavelength of 375 nm. ANS emission decays were measured with a 375 nm nanopulsed laser. The software supplied with the instrument was used to analyze emission decays. ANS emission decays across the emission spectra with a 5 nm interval were used to build decay-associated spectra (DAS). For DAS, the set of ANS emission decay curves was subjected to Global analysis, where the lifetimes were global parameters.

2.6. ANS binding to fibroin nanoparticles: deconvolution of binding curve into fluorescence lifetime species.

An aqueous solution of sfNP (1.5 μM) was titrated with 8-anilino-1-naphthalene sulfonic acid (ANS) and the steady-state fluorescence emission was measured at 490 nm. The concentration of ANS was determined using an extinction coefficient ε_{350nm}= 6300 $M^{-1}cm^{-1}$. In the steady-state measurements, the λ_{ex} and bandwidth were 340 nm and 3.5 nm, respectively. A nanopulsed LED 340nm was used for time-resolved measurements. To deconvolve ANS binding curve into fluorescence lifetime species, the emission decay measurements were performed at each point of the titration. Deconvolution and determination of dissociation constants (K_d) were performed as described in ref. [17].

RESULTS AND DISCUSSION

Far-UV CD spectrum of a freshly prepared aqueous solution of fibroin shows a single negative peak around 195 nm, characteristic of random coil conformation. The spectrum of sfNP solution exhibits drastic changes that exhibit a negative couplet characterized by peaks at 222 nm and 205 nm (Fig. 1). The spectral form is characteristic of the beta-sheet structure. Secondary structure estimation from far-UV CD spectra using the method CDSSTR has yielded 47% beta-structure, 11% turns, and 39% random coil. The random coil to beta-structure transitions has been shown in the fibroin aggregation process [6]. CR staining assay was performed to reveal the nature of the protein aggregates. The green birefringence dots were observed in the sfNP solution with CR under a polarized microscope. This observation indicates that bound CR molecules are aligned along the fiber axis, characteristic of amyloid structures. Other protein aggregates

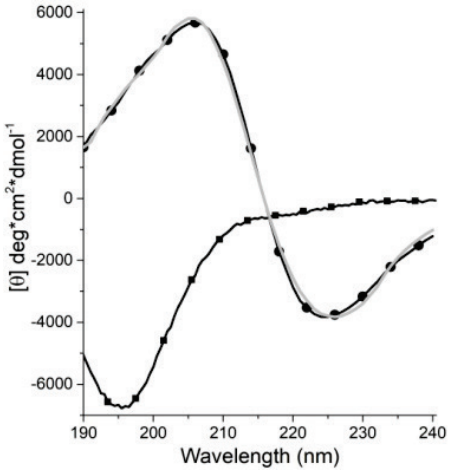

Figure 1. Far-UV CD spectra of SF solution in various states. Solid curves with square and circle symbols represent freshly prepared SF and SFNP solutions, respectively. The Gray solid curve is a calculated spectrum

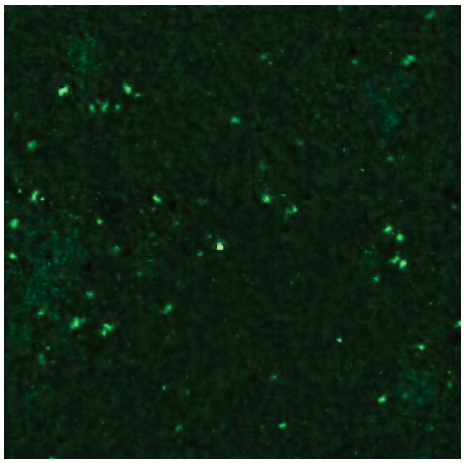

Figure 2. Birefringence image of sfNP-CR complexes

where bound CR molecules are oriented randomly do show the birefringence [18]. Therefore, data indicate that the sfNPs with an average size of about 120 nm are composed of small beta-amyloid domains.

Conformational transitions in fibroin during the sfNP formation were also evaluated with fluorescence spectroscopy. A freshly prepared aqueous solution of fibroin exhibits a fluorescence spectrum with λ_{max} of about 340 nm indicating that Trp residues are mostly localized at the surface of the protein [19]. A large blue shift from 340 nm to 324 nm is observed in the fluorescence spectrum of sfNP (Fig. 3). Consequently, during sfNP formation, Trp resides become deeply buried and are surrounded by hydrophobic sidechains [19,20]. The shoulder seen at about 360 nm is characteristic of amyloid aggregates. About 10 fold decrease in quantum yield observed in sfNP transition (from 0.056 to 0.005) indicates the location of a strong quencher group in the neighborhood of Trp residues. To verify this suggestion, acrylamide

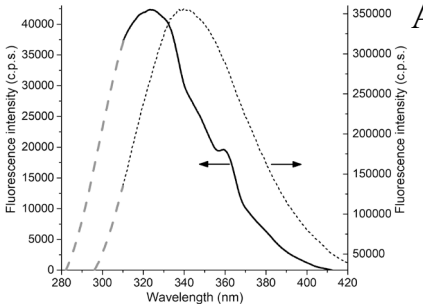

Figure 3. Trp emission spectra of SF in various states. Solid and dotted lines represent sfNP and freshly prepared SF solutions, respectively. Dashed lines were constructed from the best fit to log-normal function

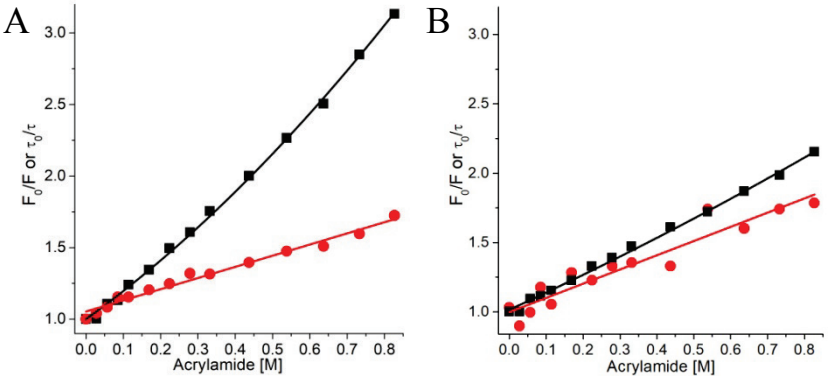

Figure 4. Steady-state and time-resolved fluorescence for acrylamide quenching of native Trp residues in SF in various states. (A) Freshly prepared SF solution. (B) fibroin solution in sfNP state. Black quares and red circles represent the quenching data from steady-state and time-resolved fluorescence, respectively

fluorescence quenching experiments were performed for fibroin in solution and NP states.

Steady-state and time-resolved fluoresce quenching by acrylamide are shown in Figure 4A. The quenching constants extracted from the global fitting (see Methods) are K_d= 0.76± 0.03 M^{-1}, k_q= 0.17x 10^9 $M^{-1}s^{-1}$ and K_s= 1.12± 0.05 M^{-1} for fibroin in solution. Both the upright curvature of F_0/F and its significant deviation from τ_0/τ are indicative of the significant contribution from static quenching. The acrylamide quenching parameters for the sfNP solution obtained from the fitting are K_d= 1.03± 0.08 M^{-1}, K_s= 0.18± 0.07 M^{-1} and k_q= 0.66 x 10^9 $M^{-1}s^{-1}$. There is an increase in the dynamic quenching constant in sfNP compared to that of fibroin solution. Both values are consistent with small solvent exposure. For comparison, fully exposed Trp residues k_q value is about 6 x 10^9 $M^{-1}s^{-1}$. In contrast, a more than 6-fold decrease is observed the static quenching in the sfNP state. Static quenching is also related to complex formation with the chromophore. Acrylamide has a very low affinity toward proteins. Therefore, significant static quenching observed at high concentrations is related to a number of acrylamide molecules vicinity of the chromophore at the moment of the excitation event. Data indicate that in sfNP formation, in contrast to fibroin solution, there is not enough space in the neighborhood Trp residues to accept the acrylamide molecules in contact distance. However, augmented dynamic quenching indicates increased mobility for some Trp residues in sfNP.

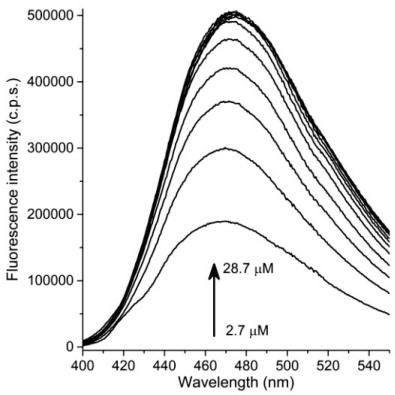

Figure 5. Fluorescence spectra of sfNP (1.5 μM) titrated with various concentrations of ANS

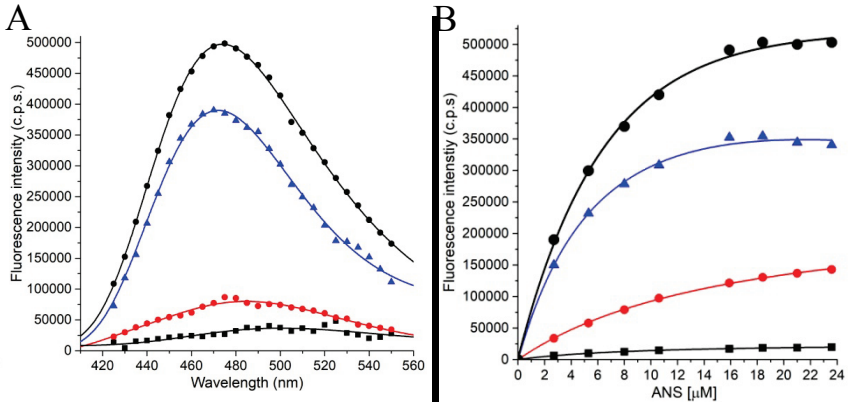

Figure 6. DAS spectra of sfNP-ANS complex and deconvolution of ANS binding curve into fluorescence lifetime species. (A) black circles- steady-steate fluorescence spectra of sfNP(1.5 μM) -ANS(28.0μM) complex; blue triangles, red circles and black squares are DAS spectrum of ANS for 14.8 ns, 4.2 ns and 0.8 ns species, respectively. (B) ANS to sfNP binding followed by fluorescence intensity. Black circles are data from steady-state fluorescence. Blue triangles, red circles and black squares are binding data for 14.8 ns, 4.2 ns and 0.8 ns species, respectively

ANS is a widely used chromophore to characterize hydrophobic patches and/or binding sites of proteins. ANS show very low fluorescence intensity with a lifetime of about 0.2 ns. A tremendous increase in fluorescence and lifetimes are observed upon binding to hydrophobic patches, the values of which depend on the dynamics of ANS and the hydrations of the sites [21,22].

The emission of ANS-SFNP complexes shows a maximum of about 474.0 nm indicative of a hydrophobic environment for ANS (Fig. 3). The emission of ANS-SFNP could be characterized by three-lifetime components 0.8 ns, 4.2 ns and 14.8 ns, each of which is characterized by individual DAS λ_{max}. To reveal the binding properties of these sites, a steady-state binding curve of ANS were deconvoluted into lifetime components (Fig. 4). The dissociation constants for ANS binding sites in SFNP were found to be 5.9±0.3 μM, 8.3±0.4 μM and 15.0±0.7 μM associated with 14.8 ns, 4.2 ns and 0.8 ns, respectively. Overall, data indicate that SFNP possesses binding sites that have distinct binding affinities, and hydrophobicity. Thus, SFNP has the potential for the delivery of drugs with various hydrophobicities.

References:

1. Hong S., Choi D.W., Kim H.N., Park C.G., Lee W., Park H.H. Protein-based nanoparticles as drug delivery systems. *Pharmaceutics*, 2020, vol. 12, no. 7, pp. 1-28.

2. Hawkins M.J., Soon-Shiong P., Desai N. Protein nanoparticles as drug carriers in clinical medicine. *Adv. Drug Deliv. Rev*., 2008., vol. 60, no. 8, pp. 876-885.

3. Weber C., Coester C., Kreuter J., Langer K. Desolvation process and surface characterisation of protein nanoparticles. *Int. J. Pharm*., 2000, vol. 194, no. 1, pp. 91-102.

4. Shao Z., Vollrath F. Surprising strength of silkworm silk. *Nature*, 2002, vol. 418, no. 6899, p. 741.

5. Suzuki Y., Yamazaki T., Aoki A., Shindo H., Asakura T. NMR study of the structures of repeated sequences, GAGXGA (X = S, Y, V), in bombyx mori liquid silk. *Biomacromolecules*, 2014, vol. 15, no. 1, pp. 104-112.

6. Gasymov O.K., Mammedzade A.M., Bakhishova M.J., Guliyeva A.J., Ragona L., Molinari H. Sodium fusidate prevents protein aggregation of silk fibroin and offers new perspectives for human lens material disaggregation. *Biophys. Chem*., 2021, vol. 279, p. 106680.

7. Zare-Zardini H., Vojdani Nejad Yazdi S., Zandian A., Zare F., Miresmaeili S.M., Dehghan-Manshadi M., Fesahat F. Synthesis, characterization, and biological evaluation of doxorubicin containing silk fibroin micro- and nanoparticles. *J. Indian Chem. Soc., Elsevier Ltd*, 2021, vol. 98, no. 10, p. 100161.

8. Giannelli M., Guerrini A., Ballestri M., Posati T., Aluigi A., Zamboni R., Sotgiu G. Bioactive Keratin and Fibroin Nanoparticles: An Overview of Their Preparation Strategies. *Nanomaterials*, 2022, vol. 12, no. 9.

9. Rockwood D.N., Preda R.C., Yucel T., Wang X., Lovett M.L., Kaplan D.L. Materials fabrication from Bombyx mori silk fibroin. *Nat Protoc*., 2011, vol. 6, no. 10, pp. 1612-1631.

10. Ragona L., Gasymov O., Guliyeva A.J., Aslanov R.B., Zanzoni S., Botta C., Molinari H. Rhodamine binds to silk fibroin and inhibits its self-aggregation. *Biochim. Biophys. Acta, Proteins Proteomics*, 2018, vol. 1866, no. 5-6, pp. 661-667.

11. Zhang Y.-Q. Preparation of Silk Fibroin Nanoparticles and Enzyme-Entrapped Silk Fibroin Nanoparticles. *Bio-Protocol*., 2018, vol. 8, no. 24, pp. 20-24.

12. Whitmore L., Wallace B.A. DICHROWEB, an online server for protein secondary structure analyses from circular dichroism spectroscopic data. *Nucleic Acids Res*., 2004, vol. 32, no. Web Server, pp. W668-W673.

13. Whitmore L., Wallace B.A. Protein secondary structure analyses from circular dichroism spectroscopy: Methods and reference databases. *Biopolymers*, 2008, vol. 89, no. 5, pp. 392-400.

14. Compton L.A., Johnson W.C. Analysis of protein circular dichroism spectra for secondary structure using a simple matrix multiplication. *Anal. Biochem*., 1986, vol. 155, no. 1, pp. 155-167.

15. Manavalan P., Johnson W.C. Variable selection method improves the prediction of protein secondary structure from circular dichroism spectra. *Anal. Biochem*., 1987, vol. 167, no. 1, pp. 76-85.

16. Antimonova O.I., Grudinina N.A., Egorov V.V., Polyakov D.S., Il'in V.V., Shavlovskii M.M. Interaction of the dye Congo red with fibrils of lysozyme, beta2-microglobulin, and transthyretin. *Cell tissue biol*., 2016, vol. 10, no. 6, pp. 468-475.

17. Gasymov O.K., Abduragimov A.R., Glasgow B.J. Evidence for internal and external binding sites on human tear lipocalin. *Arch. Biochem. Biophys*., 2007, vol. 468, no. 1, pp. 15-21.

18. Howie A.J., Brewer D.B. Optical properties of amyloid stained by Congo red: History and mechanisms. *Micron*., 2009, vol. 40, no. 3, pp. 285-301.

19. Burstein E., Vedenkina N., Ivkova M. Tryptophan Residues in Protein Molecules. *Photochem. Photobiol*., 1973, vol. 18, pp. 263-279.

20. Gasymov O.K., Abduragimov A.R., Yusifov T.N., Glasgow B.J. Site-Directed Tryptophan Fluorescence Reveals the Solution Structure of Tear Lipocalin: Evidence for Features That Confer Promiscuity in Ligand Binding. *Biochemistry*, 2001, vol. 40, no. 49, pp. 14754-14762.

21. Gasymov O.K., Glasgow B.J. ANS fluorescence: Potential to augment the identification of the external binding sites of proteins. *Biochim. Biophys. Acta*, 2007, vol. 1774, no, 3, pp. 403-411.

22. Guliyeva A.J., Gasymov O.K. ANS fluorescence: Potential to discriminate hydrophobic sites of proteins in solid states. *Biochem. Biophys. Reports*, 2020, vol. 24, no. August, p. 100843.